Unraveling the Origin of the Regioselectivity of a Supramolecular Hydroformylation Catalyst

Linnebank, P.R.; Kluwer, A.M.; Reek, J.N.H.

DOI
10.1002/cctc.202200541

Publication date
2022

Document Version
Final published version

Published in
ChemCatChem

ChemCatChem

Research Article
doi.org/10.1002/cctc.202200541

Chemistry Europe
European Chemical Societies Publishing

www.chemcatchem.org

Unraveling the Origin of the Regioselectivity of a Supramolecular Hydroformylation Catalyst

Pim R. Linnebank,[a] Alexander M. Kluwer,[b] and Joost N. H. Reek*[a, b]

Supramolecular substrate preorganization using DIMPHos ligands, which are bisphosphine ligands equipped with a carboxylate binding site, allows for control over the regioselectivity in the hydroformylation reaction. In all reported examples, the aldehyde product in which the CO was inserted farthest from the directing group, was formed in excess (for terminal alkenes the linear aldehyde). We report here an in-depth DFT study to provide mechanistic insight into this selective transformation. These calculations show large energy differences between the different hydride migration steps of competing pathways that lead to either the linear or branched aldehyde product, in line with the experimentally found selectivity. Through the use of calculated model systems of the catalyst, it is shown that the substrate binding event itself plays an important role in determining these large energy differences. Following ditopic substrate binding, the product forming pathways that lead to the minor isomeric product is particularly disfavored by the steric repulsion between the ditopically bound substrate and the apical coordinated CO ligand.

Introduction

Immense progress in the field of transition metal catalysis has been achieved in the past decades, and the number of active catalysts that have been reported is enormous. In the development of new catalysts it is important to also control the selectivity of the reaction, which nowadays has been achieved for numerous transformations.[1,2] In general, the intrinsic reactivity and substrate-biased selectivity is exploited in the catalytic reaction and optimization of the reaction conditions leads to achieve selective transformations. This approach in less effective when catalyst enables different pathways leading to different reaction products, or even worse; the desired product is formed *via* a higher reaction barrier pathway compared to a side product pathway. In these latter cases, the desired reaction product is part of a product mixture or not formed at all.

In the past two decades, supramolecular strategies in transition metal catalysis have provided chemists a toolbox to obtain selectivity control for challenging substrates as these strategies allow for energetic differentiation among competing reaction pathways.[3–13] Indeed, applying such supramolecular strategies has led to unique and unprecedented selectivity control and thus provide a complementary tool to traditional transition metal catalysts.[14–36]

One commonly explored supramolecular strategy relies on the use of bifunctional ligands that, apart from the donor atoms for coordination to the metal center, possess a recognition site for a directing group located on the substrate.[4,5,10] This strategy is commonly referred to as (supramolecular) substrate preorganization (or orientation) and is depicted schematically in Figure 1. Through binding of the directing group to the recognition site of the ligand, the reactive group is preorganized with respect to the catalytically active metal center. As a consequence, certain reaction pathways become feasible while others are not. By this way, the selectivity can be controlled in a unique manner.

A reaction in which this strategy has been applied successfully is the hydroformylation reaction, which is a transition metal catalyzed reaction where a double bond is reacted with a syngas mixture (H_2:CO) to yield an aldehyde (Figure 2).[37,38] The aldehyde can be incorporated on both sides of the double bond and often the regioselectivity of this reaction needs to be controlled. For that reason, it is important

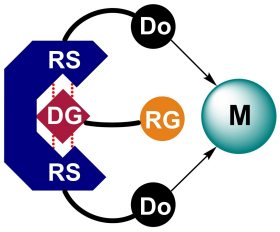

Figure 1. Schematic drawing of the concept of supramolecular substrate preorganization, M = metal center, Do = donor atom, RS = Recognition site, DG = Directing group, RG = reactive group.

[a] *Dr. P. R. Linnebank, Prof. J. N. H. Reek*
Homogeneous, Supramolecular and Bio-Inspired Catalysis
Van't Hoff Institute for Molecular Sciences University of Amsterdam
Science Park 904
1098 XH Amsterdam (The Netherlands)
E-mail: j.n.h.reek@uva.nl
[b] *Dr. A. M. Kluwer, Prof. J. N. H. Reek*
InCatT B.V.
Science Park 904
1098 XH Amsterdam (The Netherlands)

Supporting information for this article is available on the WWW under https://doi.org/10.1002/cctc.202200541

This publication is part of a joint Special Collection with EurJOC and EurJIC on the Netherlands Institute for Catalysis Research. Please see our homepage for more articles in the collection.

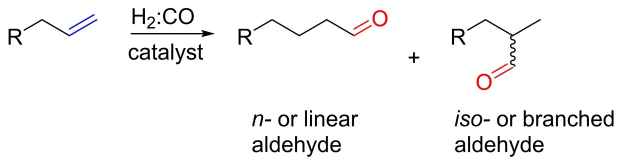

Figure 2. General reaction scheme of the hydroformylation reaction.

to understand the mechanism and know in which step the selectivity is determined.

The generally accepted mechanism, which is displayed in Figure 3, commences with the dissociation of CO from the biscarbonyl complex (**Resting state**) to generate the 16-electron species (**1**).[39–44] This is followed by alkene coordination (**2**). Subsequently, the hydride can migrate to either carbon atom of the C=C bond (*via* **ts 3**), leading to the formation either the linear or the branched rhodium-alkyl regioisomers (**4**, only linear isomer depicted) after which CO coordinates to rhodium to form (**5**). Migratory insertion of the CO generates an acyl species (**7**). Subsequent hydrogenolysis steps produces the aldehyde product (**12**) and regenerates (**1**), closing the catalytic cycle.

In general, optimization of the catalyst and the reaction conditions (e.g. ligand or syngas pressure variation) can lead to the formation of a single regioisomer with high selectivity.[23,37,45–52] However, this strategy falls short for substrates where the reactivity of the alkene is not biased to a single product or alternatively, the reactive alkene is biased to a product that is different from the desired product.[25,53–59]

Using the supramolecular substrate preorganization strategy, our group and the group of Breit *et al.* were able to control the regioselectivity of challenging substrates in the hydroformylation reaction using a carboxylate directing group.[22,26,28,33–36,60,61] The selective catalysts reported by our group were based on bisphosphine or bisphosphite ligands, coined DIMPhos, which contain a neutral anion receptor based on 7,7′-diamido-2,2′-diindolylmethane (DIM pocket) in the backbone for carboxylate binding (Figure 4).[62] For all the DIMPhos-based rhodium catalysts investigated so far, the aldehyde product that was formed was the aldehyde with the C(O)H-moiety farthest away from the directing group, i.e. for terminal alkenes the linear aldehyde was the dominant product. This phenomenon was exploited for 2-carboxyvinylarenes, which are converted the linear (outermost) aldehyde product, overruling the typical natural branched selectivity of these compounds.[27,60] We recently reported the regioselective conversion of the internal double bond of natural fatty acids using this substrate preorganization approach, in which the distance between the carboxylic acid directing group and the internal alkene reactive group was eight bonds.[33]

Preliminary calculations combined with mechanistic studies show that the regioselectivity for these catalysts is determined in the hydride migration step of the catalytic cycle (Figure 3).[22,26] Ditopic substrate binding restricts alkene rotation, which leads to hydride migration to the C2 carbon atom and, in the case of terminal alkenes, yields to the linear aldehyde product as can be seen in **ts 3** in Figure 5.[22,26] However, the reason why the hydride migration transition state toward the linear product is significantly lower in energy compared to the competing hydride migration transition state is not well understood. For other hydroformylation catalysts, in-depth DFT calculations have resulted in improved understanding of these catalysts and therefore we set out to investigate this phenom-

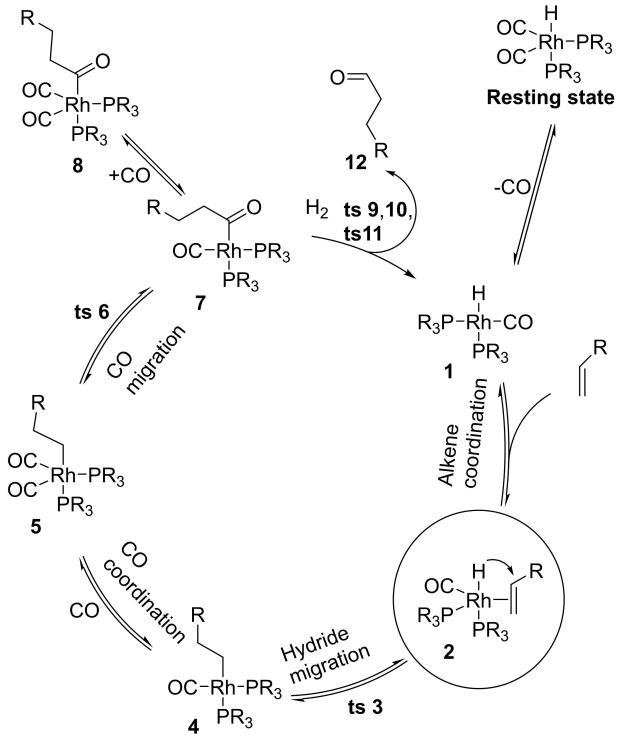

Figure 3. General hydroformylation catalytic cycle (Heck-Breslow mechanism).

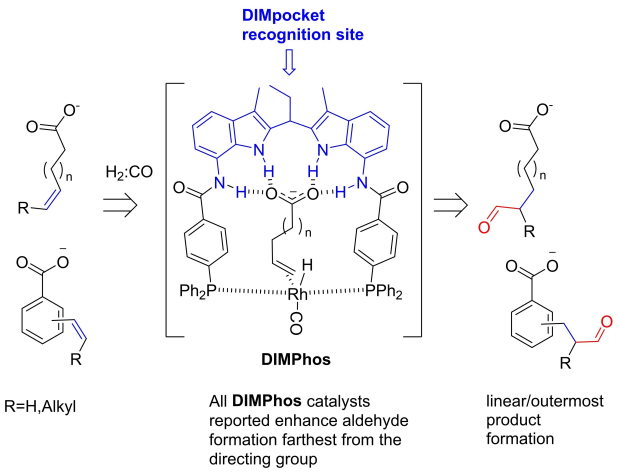

Figure 4. Supramolecular substrate preorganization using [Rh(DIMPhos]-catalyst in hydroformylation reaction yielding the aldehyde product with the CO function farthest from the carboxylic acid *i.e.* the linear product for terminal alkenes.

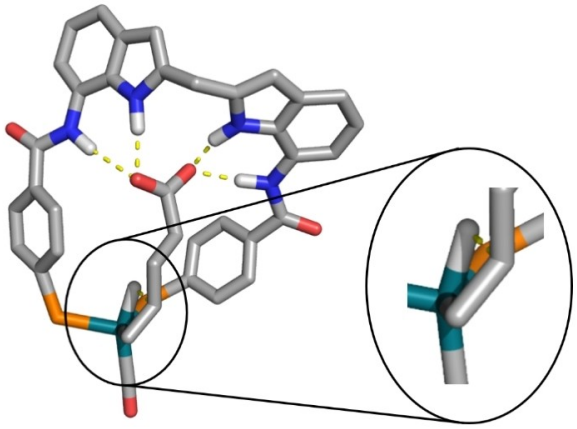

Figure 5. Restricted rotation of the alkene substrate as calculated for (**ts 3^{D}**) leads to control of the selectivity determining hydride migration step.

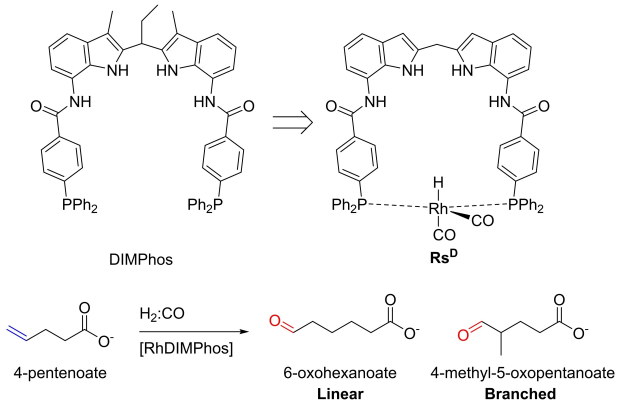

Figure 7. The DIMPHos ligand, and the simplified [Rh(DIMPhos)] system studied by DFT calculations in the resting state (**Rs^{D}**); conversion of 4-pentenoate to provide 6-oxohexanoate in high selectivity when using DIMPhos based catalysts. Only a small amount of 4-methyl-5-oxopentanoate is formed.

enon using DFT calculations[63–76] In this contribution we report a theoretical study to unravel the mechanistic basis that explains the regioselectivity that is typically observed for the DIMPhos based rhodium catalysts.

Results and Discussion

To investigate the mechanistic basis for the observed regioselectivity, the reaction profile of the DIMPhos catalyst was analyzed using DFT calculations.

The ADF modeling suite was used with BLYP–D3BJ as a functional, DZP as a basis set for all atoms apart from rhodium, for which a TZP basis set was used. [77] Furthermore, we used ZORA to account for relativistic effects. [78] The ligand system used for the calculation is a simplified version of bis(4-(diphenylphosphino)benzoamide) of 1,1-bis-(-7-amino-3-methyl-1H-indol-2-yl)-propane), coined DIMPhos, (Figure 7).[22,26,60] This simplification is justified as it involves removal of alkyl groups remote from the catalyst.

With the simplified [Rh(DIMPhos)(CO)$_2$(H)] (**Rs^{D}**) complex, we calculated the catalytic pathway of the hydroformylation reaction of 4-pentenoate, a substrate that is converted with high regioselectivity. The substrate exactly spans the distance between the carboxylate receptor and the rhodium metal center of this catalyst. The DFT calculated energy profile of the conversion of 4-pentenoate to 6-oxohexanoate is reported in Figure 6. The reaction commences with CO dissociation from [Rh((4-pentanoate) ⊂ DIMPhos) (CO)$_2$(H)] (**Rs^{D}** ⊂ (**pentenoate**)) in which the superscript "D"denotes the DIMPhos ligand) directly followed by the alkene coordination (**2^{D}**) that is already bound to the anion binding pocket. This is followed by a hydride migration step (**ts 3^{D}**). The combination of these

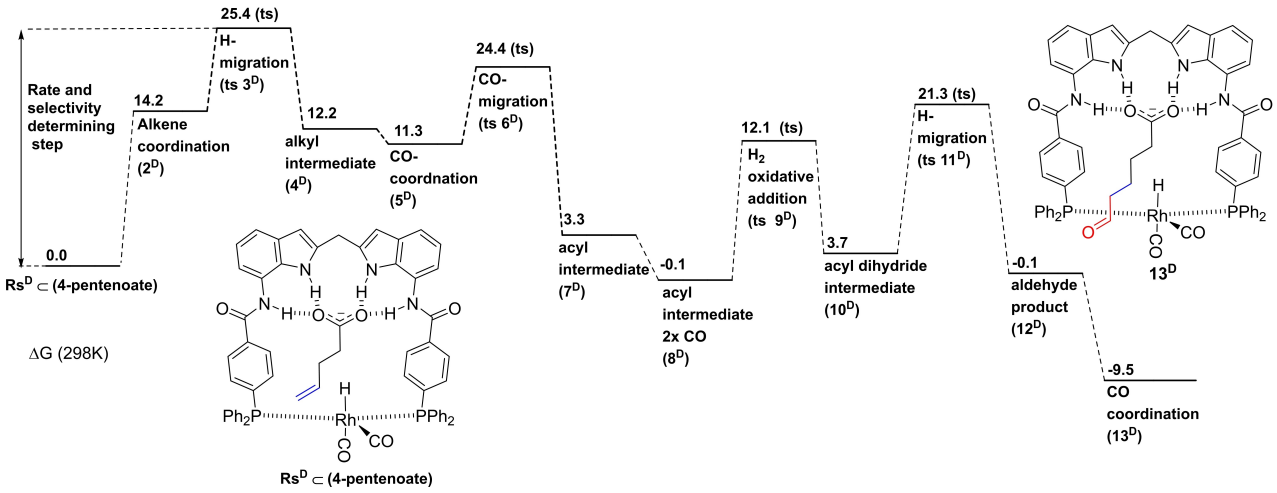

Figure 6. Lowest energy pathway of the hydroformylation of 4-pentenoate to 6-oxohexanoate using [Rh((4-pentenoate) ⊂ DIMPhos) (CO)$_2$(H)]. In this figure, only the lowest calculated energetic minima, intermediates and relevant transition states are displayed for clarity. The superscript (D) denotes the DIMPhos ligand ligated complex. Note: Following CO dissociation, the alkene immediately coordinates to the rhodium and no **1^{D}**⊂ (4-pentenoate) species is identified.

aforementioned steps (2^D and **ts** 3^D) represents the highest energetic barrier for this reaction pathway, which make these steps rate and selectivity determining. This is consistent with previously reported mechanistic studies on this system.[22,26]

For the later steps, significantly lower energetic barriers are obtained and therefore these do not affect the regioisomeric outcome of the reaction (see supporting info). The regioselectivity is determined during the hydride migration step from 2^D via transition state **ts** 3^D leading to the alkyl intermediate 4^D. The branched transition states are significantly higher than the lowest linear transition state (3.9 and 15.9 kcal/mol), which forms the basis for the high regioselectivity (Figure 8).

Interestingly, prior to the coordination of 4-pentenoic acid, only minor energy differences are observed (Figure 9). This shows that the energetic differentiation that determines the regioselectivity is not present prior to substrate coordination. As a result we further investigated the alkene coordination 2^D and subsequent hydride migration **ts** 3^D steps.

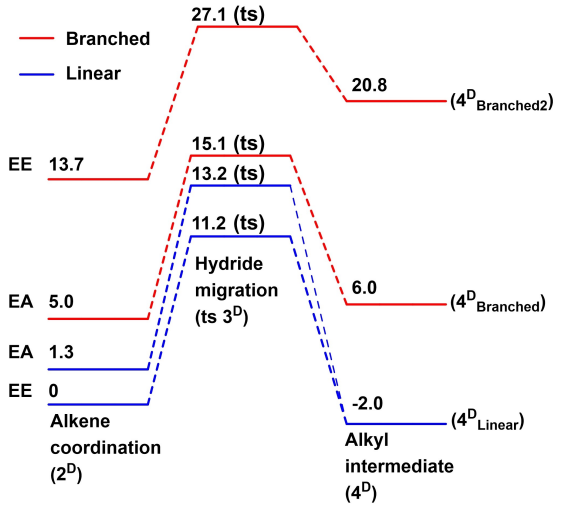

Figure 8. Overview of calculated competing hydride migration pathways. Blue pathways are linear-product forming. Red pathways are branched-product forming. Energies are normalized by subtracting the energy from the lowest energy [Rh((4-pentenoate) ⊂ DIMPhos)(CO)(H)] structure (2^D). EE denotes the equatorial-equatorial orientation of the phosphines. EA denotes the equatorial-apical orientation of the phosphines

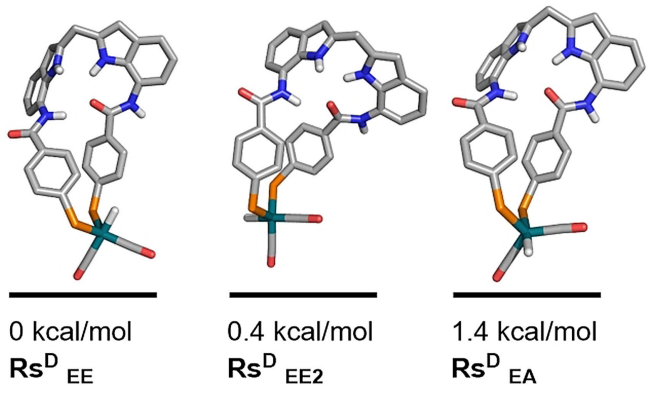

Figure 9. [Rh (DIMPhos) $(CO)_2(H)$] Rs^D complex energies normalized against the lowest energy [Rh (DIMPhos) $(CO)_2(H)$] geometry $\mathbf{Rs}^D_{EE}$. All energies in kcal/mol. Some hydrogens and phenyls groups are removed for clarity, but are included in the calculations. Minor relative energy differences observed for different coordination modes

The four alkene coordination geometries for intermediate (2^D) that were obtained from our calculations are displayed in Figure 10, and are indicated EE pre linear, EE pre branched (EE stands for equatorial-equatorial coordination of bidentate phosphorus ligand) and EA pre linear, EA pre branched (EA stands for equatorial-axial coordination of bidentate phosphorus ligand). The coordination geometry (EE vs EA) in the ground state (2^D) remains the same in the following transition states (**ts** 3^D).[66] The overall geometries of the **ts** 3^D are highly similar to the associated 2^D ground state structures. Following hydride migration, three alkyl intermediates (4^D) are obtained. One linear alkyl intermediate (4^D_{Linear}) and two branched alkyl intermediates ($4^D_{Branched}$ and $4^D_{Branched2}$), as the two pre linear transition states lead to an identical linear alkyl intermediate. The alkyl intermediate 4^D_{Linear} that leads to the linear aldehyde is lowest in energy (−2.0 kcal/mol). The two branched transition states yields to two different alkyl intermediates, with the lowest energy branched transition state also leading to the lowest branched alkyl intermediate. The two branched alkyl intermediates ($4^D_{Branched}$ and $4^D_{Branched2}$), which differ in the position of the CO, the structure with the CO pointing to the DIM pocket is highest in energy (20.8 kcal/mol for $4^D_{Branched2}$).

From initial inspection, it is not clear what causes the energetic differences between the 2^D structures and the subsequent **ts** 3^D transition states. The two EE geometries that lead to the branched ($2^D_{EE\ pre\ branched}$) or the linear ($2^D_{EE\ pre\ linear}$) product differ in the relative position of the CO and hydride at the axial position, which are inverted. This inversion of the CO and hydride positions leads to a large energy difference of 13.7 kcal/mol. The $2^D_{EA\ pre\ linear}$ is only slightly higher in energy than the lowest EE geometry (1.3 kcal/mol), whereas the $2^D_{EA\ pre\ branched}$ is 5.0 kcal/mol higher in energy and therefore most likely not formed. The EE and EA structures were compared to a [$Rh(PPh_3)(CO)(H)$] model system (see supporting information, Table 5). This analysis shows that the $2^D_{EE\ pre\ linear}$ and $2^D_{EA\ pre\ linear}$ structures adopt a less strained structure than the $2^D_{EE\ pre\ branched}$ and $2^D_{EA\ pre\ branched}$ structures. For intermediates 2^D and 4^D and transition state **ts** 3^D the structures with CO pointing to the DIM pocket are energetically unfavorable. In contrast, when the CO points to the DIM pocket ($\mathbf{RS}^D_{EE2}$, see Figure 9), the energy is only 0.4 kcal/mol higher than the lowest energy geometry in which the hydride points to the pocket.

These results show that the substrate binding event is responsible for the large differences in energy when the CO and H ligands are inverted in **2** and transition state **ts 3**, which in turn is the origin of the high regioselectivity (Figure 11). Therefore, we studied the effect of the substrate binding event on the relative rhodium geometries in detail. The ditopic substrate binding event involves CO dissociation/alkene coordination to the rhodium center as well as carboxylate binding in the DIM pocket (Figure 11). To investigate the effect of both binding events on the energetic differentiation separately, we replaced the 4-pentenoate moiety with a propene or CO moiety

Research Article
doi.org/10.1002/cctc.202200541
Chemistry Europe
European Chemical Societies Publishing

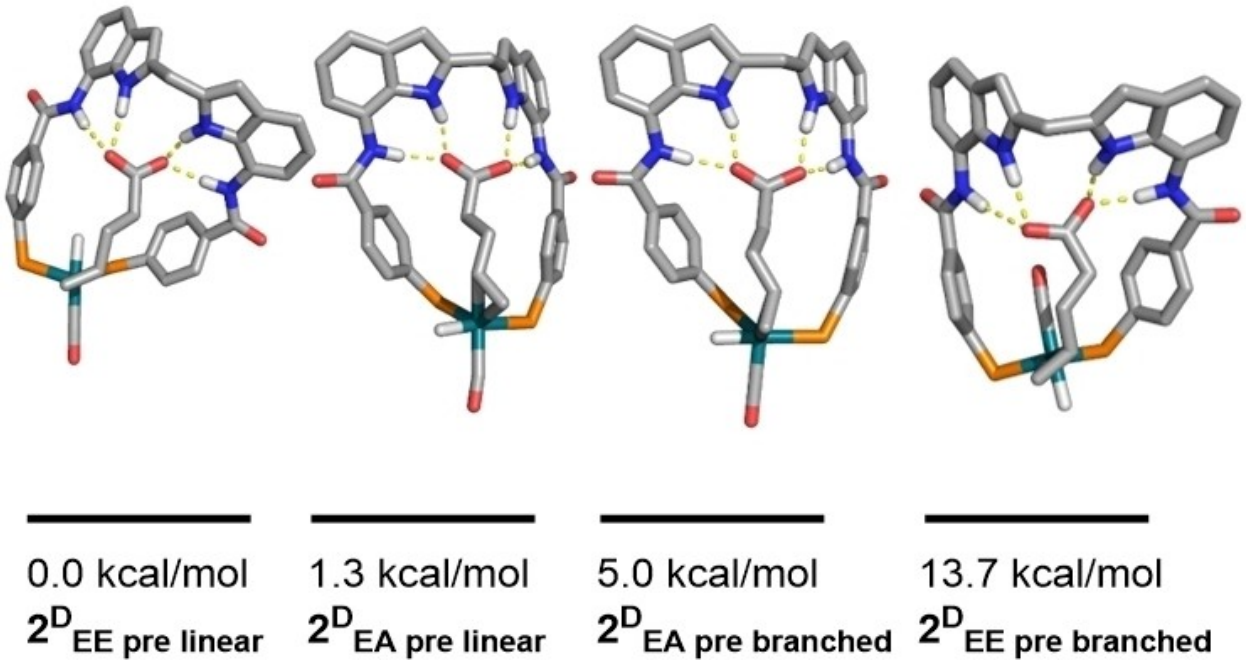

Figure 10. Four ground state geometries of [Rh((4-pentenoate) ⊂ DIMPhos)(CO)(H)] (2^D) Energies normalized by subtracting the energy from the lowest energy $2^D_{\text{EE pre linear}}$ structure. Some hydrogens and phenyls are removed for clarity, but are included in the calculations. For explanation of labels, see text

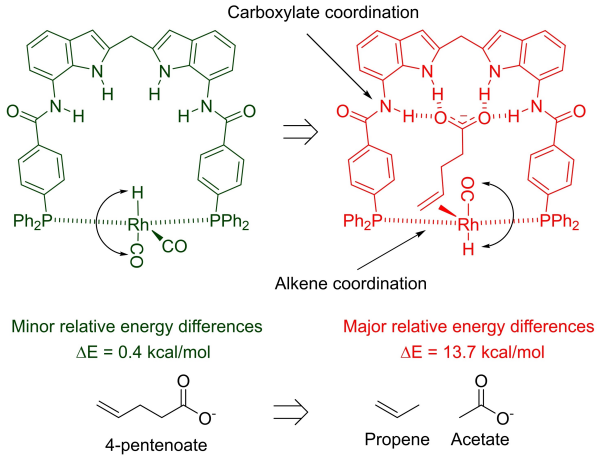

Figure 11. Ditopic binding of 4-pentenoate to the RhDIMPhos binding in the DIM pocket appears responsible for the large energy differences between the different coordination modes ($\mathbf{Rs}^D$ to 2^D (⊂ 4-pentenoate)). Inversion of the position of the CO and the hydride results in low energy differences (△E) in absence of 4-pentenoate and high energy differences in the presence of ditopically bound 4-pentenoate. Propene and acetate moieties are used as model systems for ditopic binding of 4-pentenoate to study the origin of the energetic differentiation.

that coordinates to rhodium or an acetate moiety that binds in the DIM pocket (Figure 12). Alternatively, the 4-pentenoate moiety was replaced by both a propene or CO ligand and an acetate moiety to model the ditopic binding (Figure 12). This allows us to systematically study the effects of both binding events on the relative energy of various systems with the ligand in the EE and EA coordination modes.

We calculated the four coordinate 1^D Rh(DIMPhos) structure and the analogous structure with an acetate bound in the DIM pocket (**1** (⊂acetate)) (Figure 12). We also calculated five coordinate Rh(DIMPhos) structures with a single hydride ligand and a two CO ligands ($\mathbf{Rs}^D$) as well as the Rh(DIMPhos) structures with a single hydride ligand, a single CO ligand and a single propene ligand coordinated to rhodium ($2^{D\ \text{Propene}}$). Again, the analogous structures of $\mathbf{Rs}^D$ and $2^{D\ \text{Propene}}$ were calculated in presence of an acetate in the DIMPocket ($\mathbf{Rs}^D$ (⊂acetate) and 2^{D}_{propene} (⊂acetate)). We have compared the energy differences between the various coordination modes around rhodium of these abovementioned structures. For all structures in which rhodium is four coordinate (1^D and 1^D (⊂acetate))], the lowest energy structure was obtained when the phosphines adopt a *cis* conformation. For the optimized geometry where the phosphines adopt a *trans* conformation, the energy was slightly higher than the *cis* analogue (0.9–3.1 kcal/mol). Interestingly, minor energy differences are observed between the two trans coordination geometries around rhodium where the CO and hydride are inverted (0.1–0.6 kcal/mol), whereas the [Rh((4-pentenoate) ⊂ DIMPhos)(CO)(H)] (2^D) (*vide supra*) displays large differences in energy when the CO and hydride positions are inverted ($2^D_{\text{EE pre linear}}$ and $2^D_{\text{EE pre branched}}$).

For all pentacoordinate complexes calculated, the lowest energy geometries were structures where the phosphines adopted an EE conformation. The EA geometries were 1.4–3.4 kcal/mol higher than the lowest EE geometry, similar to what is observed with $2^D_{\text{EE pre linear}}$ and $2^D_{\text{EA pre linear}}$ (*vide supra*). For complexes $\mathbf{Rs}^D$ and $2^{D\ \text{Propene}}$ no large energy differences are observed between the structures where the CO points to the DIM pocket and the hydride points to the DIM pocket. Only

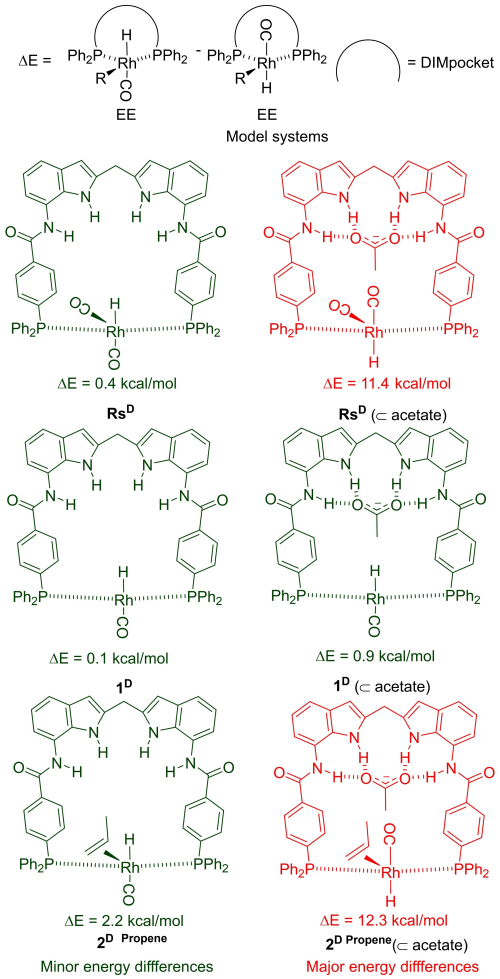

Figure 12. Model systems studied. For all structures the EE geometries were calculated and the energy differences (△ E) are presented between the EE structures where the position of the hydride and CO ligands are inverted. Only when acetate is bound and rhodium is five coordinate, a high energy intermediate is obtained where the phosphines adopt an EE conformation and CO points to the DIM pocket, which is the case for **Rs**^{D} (⊂acetate) and **2**$^{D\ Propene}$ (⊂acetate). These high energy complexes were colored red for clarity.

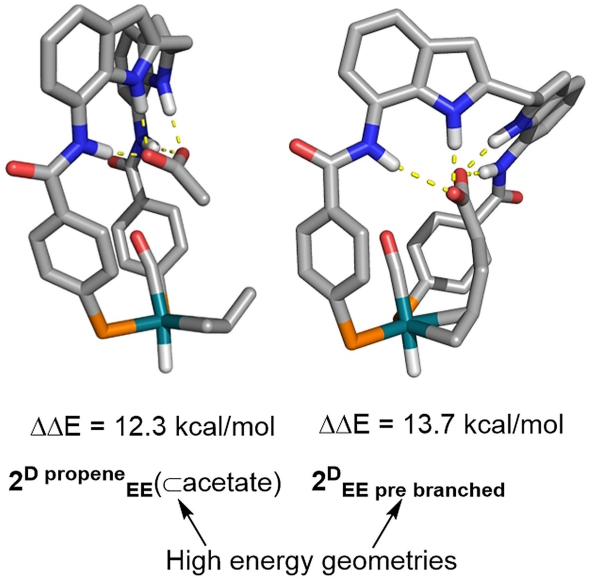

Figure 13. Structural similarity between the **2**$^{D}_{EE\ pre\ branched}$ geometry where the CO points to the DIM pocket and the high energy **2**$^{D\ Propene}$(⊂acetate) where the CO adopts a similar orientation relative to rhodium and the carboxylate moiety. △△Energies determined by subtracting the energy outcome from the lowest energy **2**$^{D}_{EE\ pre\ linear}$ structure and the **2**^{Propene}-(⊂acetate) structure respectively. Some hydrogens and phenyls have been omitted for clarity, but are included in the calculations

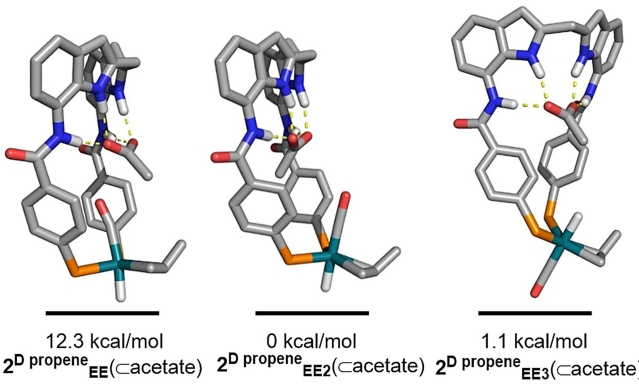

Figure 14. **2**$^{D\ Propene}$ (⊂acetate) identified EE ground state geometries. All energies were normalized to the lowest identified energetic **2**$^{D\ Propene}_{EE2}$ (⊂acetate) geometry. All energies in kcal/mol^{-1}. Some hydrogens and phenyls have been omitted for clarity, but are included in the calculations.

when the acetate is bound in the pocket and rhodium is pentacoordinate; i.e. for **Rs** (⊂acetate) and **2**^{Propene} (⊂acetate) a high energy intermediate in which the CO points to the DIM pocket was obtained (11.4–12.3 kcal/mol) (Figure 12; structures are indicated in red). This high energy intermediate where CO points to the DIMpocket for **Rs** (⊂acetate) and **2**^{Propene} (⊂acetate) is structurally similar to the high **2**$^{D}_{EE\ pre\ branched}$ species (Figure 13), where a pathway to the branched aldehyde product is hindered. This shows the complexity of the system, as the carboxylate binding event has an influence on the different coordination geometries around the rhodium metal of the [Rh((4-pentenoate) ⊂ DIMPhos)(CO)(H)] **2**^{D} complex, and these in turn lead to disfavoring of some of the competing branched product forming pathways.

We also identified a low energy **2**$^{D\ Propene}$ (⊂acetate) structure in which the CO points to the DIM pocket (Figure 14, **2**$^{D\ Propene}_{EE2}$(⊂acetate)). However, for this structure the acetate is oriented away from the propene moiety and such structure cannot be formed for ditopically bound substrates. When the acetate is placed in close proximity to the propene moiety (Figure 14, **2**$^{D\ Propene}_{EE}$ (⊂acetate), the energy is significantly higher (12.3 kcal/mol). Importantly, if the CO moiety points to the DIM pocket in these structures, it experiences steric hindrance with the acetate moiety which leads to the relative high energy of these structures.

The model structures of **2**$^{D\ Propene}_{EE}$(⊂acetate) and **2**$^{D\ Propene}_{EE2}$(⊂acetate) with the acetate orientated in different manners, clearly show why the analogous **2**$^{D}_{EE\ pre\ branched}$ structure is high in

energy. With 4-pentenoate, the carboxylate and propene are covalently linked and therefore are in close proximity by default, which leads to steric hindrance between the 4-pentenoate moiety and the CO ligand which points to the DIM-pocket. This steric clash forms the basis for the high energy of this pre branched structure and as a result, the catalyst adopts preferably the $2^{D}_{EE\ pre\ linear}$ geometry upon ditopic substrate binding as this geometry is significantly lower in energy. Hence the linear aldehyde product is produced specifically.

These results taken together show that the substrate binding event is responsible for the energy differences between the relative ligand orientations around rhodium, which forms the basis for the regioselectivity observed. To accommodate the substrate in a ditopic fashion, the catalyst predominantly adopts an orientation where the phosphines bind in an EE conformation that preorganizes the substrate to the linear/outermost product. The substrate hampers the EE branched pathway due to steric clash between the substrate and the CO ligand (Figure 15). Furthermore, the substrate binding event also results in higher energy differences between the lowest energy EE orientation and the EA geometries in the selectivity determining step, as prior to substrate binding, only minor energy differences are observed between the complexes with different ligand geometries.

Conclusions

In summary, we have investigated the mechanistic basis of a hydroformylation catalyst that derives its selectivity through supramolecular substrate preorganization. When this catalyst converts terminal alkenes with a carboxylate directing group, the linear product is formed. DFT calculations show that the substrate and the CO moiety experience steric hindrance in a branched product forming pathway. Also the alternative branched product forming pathway in which the phosphines adopt an EA coordination geometry around rhodium is also significantly higher than the linear product forming pathways. Interestingly, both the alkene binding event as well as the carboxylate binding event themselves are important for creating energy differences between different species. The detailed mechanism of this reaction is therefore more complex than originally anticipated.

We envision that these results pave the way for the design of new ligands that operate on the same principle, but are able to bind other directing groups. Moreover, these results suggest that catalysts based on other receptors than the previously reported 7,7′-diamido-2,2′-diindolylmethane should also be able to control the regioselectivity in an analogous manner. Furthermore, these results show that the steric clash of the substrate with the CO moiety disfavors the formation of the branched product, explaining the success of DIMPhos ligands to obtained these type of selectivities. Substrate preorganization at catalyst centers that favor the opposite aldehyde product should be based on a rather different design than was used for the DIMPhos ligand class. Using these insights, we are currently conducting experiments in our pursuit of novel catalysts that operate on the basis of substrate preorganization in our laboratories.

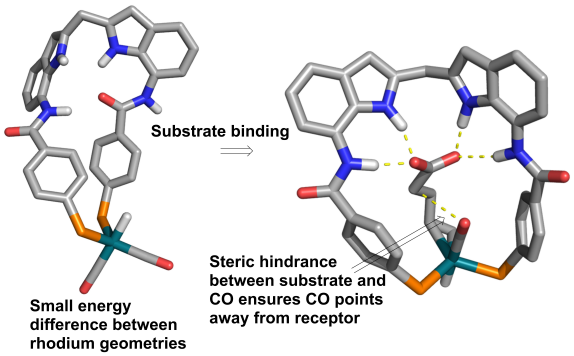

Figure 15. Conceptual explanation for large difference between rhodium geometries upon substrate binding. Energy differences caused by substrate binding, reminiscent of induced fit effects commonly observed in enzymatic catalysis.

Computational details

All DFT calculations were performed with the Amsterdam Density Functional[77,79] (ADF) program. The BLYP–D3(BJ)[80,81] density functional was used together with a small core DZP basis set. Relativistic effects were accounted for by running calculations with zeroth-order regular approximation (ZORA).[81] All local minima were characterized by having zero imaginary frequencies after running a frequency calculation. All transition states were characterized by having one imaginary frequency.

Acknowledgements

NWO, the Dutch science foundation, is acknowledged for financial support. We also would like to thank InCatT for financial support.

Conflict of Interest

The authors declare no conflict of interest.

Data Availability Statement

The data that support the findings of this study are available from the corresponding author upon reasonable request.

Keywords: DFT calculations · Hydroformylation · Regioselectivity · Substrate preorganization · Supramolecular catalysis

[1] P. W. N. M. van Leeuwen, *Homogeneous Catalysis: Understanding the Art*, Springer Netherlands, Dordrecht, **2004**.
[2] M. Beller, C. Bolm, *Transition Metals for Organic Synthesis*, Wiley- VCH, Weinheim, **2004**.
[3] F. D. Toste, M. S. Sigman, S. J. Miller, *Acc. Chem. Res.* **2017**, *50*, 609–615.
[4] D. Vidal, G. Olivo, M. Costas, *Chem. Eur. J.* **2018**, *24*, 5042–5054.

[5] S. H. A. M. Leenders, R. Gramage-Doria, B. De Bruin, J. N. H. Reek, *Chem. Soc. Rev.* **2015**, *44*, 433–448.
[6] S. S. Nurttila, P. R. Linnebank, T. Krachko, J. N. H. Reek, *ACS Catal.* **2018**, *8*, 3469–3488.
[7] M. Raynal, P. Ballester, A. Vidal-Ferran, P. W. N. M. van Leeuwen, *Chem. Soc. Rev.* **2014**, *43*, 1660–1733.
[8] M. Raynal, P. Ballester, A. Vidal-Ferran, P. W. N. M. van Leeuwen, *Chem. Soc. Rev.* **2014**, *43*, 1734–1787.
[9] J. Meeuwissen, J. N. H. Reek, *Nat. Chem.* **2010**, *2*, 615–621.
[10] P. Dydio, J. N. H. Reek, *Chem. Sci.* **2014**, *5*, 2135–2145.
[11] H. J. Davis, R. J. Phipps, *Chem. Sci.* **2017**, *8*, 864–877.
[12] A. Fanourakis, P. J. Docherty, P. Chuentragool, R. J. Phipps, *ACS Catal.* **2020**, *10*, 10672–10714.
[13] P. W. N. M. van Leeuwen, *Supramolecular Catalysis*, Wiley-VCH: Weinheim, **2008**.
[14] H. J. Davis, M. T. Mihai, R. J. Phipps, *J. Am. Chem. Soc.* **2016**, *138*, 12759–12762.
[15] G. Olivo, G. Farinelli, A. Barbieri, O. Lanzalunga, S. Di Stefano, M. Costas, *Angew. Chem. Int. Ed.* **2017**, *56*, 16347–16351.; *Angew. Chem.* **2017**, *129*, 16565–16569.
[16] G. Olivo, G. Capocasa, B. Ticconi, O. Lanzalunga, S. Di Stefano, M. Costas, *Angew. Chem. Int. Ed.* **2020**, *59*, 12703–12708.; *Angew. Chem.* **2020**, *132*, 12803–12808.
[17] Y. Y. Kuninobu, H. Ida, M. Nishi, M. Kanai, *Nat. Chem.* **2015**, *7*, 712–717.
[18] S. Das, C. D. Incarvito, R. H. Crabtree, G. W. Brudvig, *Science* **2006**, *312*, 1941–1943.
[19] A. Bauer, F. Westkämper, S. Grimme, T. Bach, *Nature* **2005**, *436*, 1139–1140.
[20] P.-A. R. Breuil, F. W. Patureau, J. N. H. Reek, *Angew. Chem. Int. Ed.* **2009**, *48*, 2162–2165.; *Angew. Chem.* **2009**, *121*, 2196–2199.
[21] S. Bai, C. B. Bheeter, J. N. H. Reek, *Angew. Chem. Int. Ed.* **2019**, *58*, 13039–13043.; *Angew. Chem.* **2019**, *131*, 13173–13177.
[22] P. Dydio, W. I. Dzik, M. Lutz, B. de Bruin, J. N. H. Reek, *Angew. Chem. Int. Ed.* **2011**, *50*, 396–400. *Angew. Chem.* **2011**, *123*, 416–420.
[23] V. F. Slagt, J. N. H. Reek, P. C. J. Kamer, P. W. N. M. Van Leeuwen, *Angew. Chem. Int. Ed.* **2001**, *40*, 4271–4274.; *Angew. Chem.* **2001**, *113*, 4401–4404.
[24] V. F. Slagt, P. C. J. Kamer, P. W. N. M. Van Leeuwen, J. N. H. Reek, *J. Am. Chem. Soc.* **2004**, *126*, 1526–1536.
[25] M. Kuil, T. Soltner, P. W. N. M. Van Leeuwen, J. N. H. Reek, *J. Am. Chem. Soc.* **2006**, *128*, 11344–11345.
[26] P. Dydio, R. J. Detz, J. N. H. Reek, *J. Am. Chem. Soc.* **2013**, *135*, 10817–10828.
[27] P. Dydio, J. N. H. Reek, *Angew. Chem. Int. Ed.* **2013**, *52*, 3878–3882.; *Angew. Chem.* **2013**, *125*, 3970–3974.
[28] P. Dydio, M. Ploeger, J. N. H. Reek, *ACS Catal.* **2013**, *3*, 2939–2942.
[29] T. A. Bender, R. G. Bergman, K. N. Raymond, F. D. Toste, *J. Am. Chem. Soc.* **2019**, *141*, 11806–11810.
[30] J. Daubignard, R. J. Detz, A. C. H. Jans, B. de Bruin, J. N. H. Reek, *Angew. Chem. Int. Ed.* **2017**, *56*, 13056–13060.; *Angew. Chem.* **2017**, *129*,13236–13240.
[31] P. Fackler, C. Berthold, F. Voss, T. Bach, *J. Am. Chem. Soc.* **2010**, *132*, 15911–15913.
[32] P. Fackler, S. M. Huber, T. Bach, *J. Am. Chem. Soc.* **2012**, *134*, 12869–12878.
[33] P. R. Linnebank, S. F. Ferreira, A. M. Kluwer, J. N. H. Reek, *Chem. Eur. J.* **2020**, *26*, 8214–8219.
[34] T. Šmejkal, B. Breit, *Angew. Chem. Int. Ed.* **2008**, *47*, 311–315. *Angew. Chem.* **2008**, *120*, 317–321.
[35] T. Šmejkal, D. Gribkov, J. Geier, M. Keller, B. Breit, *Chem. Eur. J.* **2010**, *16*, 2470–2478.
[36] W. Fang, B. Breit, *Angew. Chem. Int. Ed.* **2018**, *57*, 14817–14821.; *Angew. Chem.* **2018**, *130*, 15033–15037.
[37] R. Franke, D. Selent, A. Börner, *Chem. Rev.* **2012**, *112*, 5675–5732.
[38] P. W. N. M. van Leeuwen, C. P. Casey, G. T. Whiteker, *Rhodium Catalyzed Hydroformylation*, Kluwer Academic Publishers, Dordrecht, **2000**.
[39] R. F. Heck, D. S. Breslow, *J. Am. Chem. Soc.* **1961**, *83*, 4023–4027.
[40] R. F. Heck, *Acc. Chem. Res.* **1969**, *2*, 10–16.
[41] A. C. Brezny, C. R. Landis, *J. Am. Chem. Soc.* **2017**, *139*, 2778–2785.
[42] E. R. Nelsen, A. C. Brezny, C. R. Landis, *J. Am. Chem. Soc.* **2015**, *137*, 14208–14219.
[43] A. L. Watkins, C. R. Landis, *J. Am. Chem. Soc.* **2010**, *132*, 10306–10317.
[44] C. Kubis, M. Sawall, A. Block, K. Neymeyr, R. Ludwig, A. Börner, D. Selent, *Chem. A Eur. J.* **2014**, *20*, 11921–11931.
[45] P. C. J. Kamer, P. W. N. M. Van Leeuwen, J. N. H. Reek, *Acc. Chem. Res.* **2001**, *34*, 895–904.
[46] C. P. Casey, E. Lin Paulsen, E. W. Beuttenmueller, B. R. Proft, L. M. Petrovich, B. A. Matter, D. R. Powell, *J. Am. Chem. Soc.* **1997**, *119*, 11817–11825.
[47] C. P. Casey, G. T. Whiteker, M. G. Melville, L. M. Petrovich, J. A. Gavney, D. R. Powell, *J. Am. Chem. Soc.* **1992**, *114*, 5535–5543.
[48] A. Phanopoulos, K. Nozaki, *ACS Catal.* **2018**, *8*, 5799–5809.
[49] G. M. Noonan, J. A. Fuentes, C. J. Cobley, M. L. Clarke, *Angew. Chem. Int. Ed.* **2012**, *51*, 2477–2480.; Angew. Chem. **2012**, 2527–2530.
[50] S. Yu, Y. M. Chie, Z. H. Guan, Y. Zou, W. Li, X. Zhang, *Org. Lett.* **2009**, *11*, 241–244.
[51] J. Wildt, A. C. Brezny, C. R. Landis, *Organometallics* **2017**, *36*, 3142–3151.
[52] L. Iu, J. A. Fuentes, M. E. Janka, K. J. Fontenot, M. L. Clarke, *Angew. Chem. Int. Ed.* **2019**, *58*, 2120–2124. *; Angew. Chem.* **2019**, *131*, 2142–2146.
[53] T. E. Lightburn, M. T. Dombrowski, K. L. Tan, *J. Am. Chem. Soc.* **2008**, *130*, 9210–9211.
[54] C. U. Grünanger, B. Breit, *Angew. Chem. Int. Ed.* **2008**, *47*, 7346–7349.; *Angew. Chem.* **2008**, 7456–7459.
[55] C. U. Grünanger, B. Breit, *Angew. Chem. Int. Ed.* **2010**, *49*, 967–970.
[56] X. Sun, K. Frimpong, K. L. Tan, *J. Am. Chem. Soc.* **2010**, *132*, 11841–11843.
[57] Y. Ueki, H. Ito, I. Usui, B. Breit, *Chem. Eur. J.* **2011**, *17*, 8555–8558.
[58] A. D. Worthy, C. L. Joe, T. E. Lightburn, K. L. Tan, *J. Am. Chem. Soc.* **2010**, *132*, 14757–14759.
[59] C. L. Joe, T. P. Blaisdell, A. F. Geoghan, K. L. Tan, *J. Am. Chem. Soc.* **2014**, *136*, 8556–8559.
[60] P. Dydio, R. J. Detz, B. de Bruin, J. N. H. Reek, *J. Am. Chem. Soc.* **2014**, *136*, 8418–8429.
[61] S. T. Bai, V. Sinha, A. M. Kluwer, P. R. Linnebank, Z. Abiri, B. de Bruin, J. N. H. Reek, *ChemCatChem* **2019**, *11*, 5322–5329.
[62] P. Dydio, T. Zieliński, J. Jurczak, *Chem. Commun.* **2009**, 4560–4562.
[63] V. Bocokić, A. Kalkan, M. Lutz, A. L. Spek, D. T. Gryko, J. N. H. Reek, *Nat. Commun.* **2013**, *4*, 1–9.
[64] M. Kumar, R. V. Chaudhari, B. Subramaniam, T. A. Jackson, *Organometallics* **2014**, *33*, 4183–4191.
[65] M. Kumar, R. V. Chaudhari, B. Subramaniam, T. A. Jackson, *Organometallics* **2015**, *34*, 1062–1073.
[66] I. Jacobs, B. De Bruin, J. N. H. Reek, *ChemCatChem* **2015**, *7*, 1708–1718.
[67] P. Dingwall, J. A. Fuentes, L. Crawford, A. M. Z. Slawin, M. Bühl, M. L. Clarke, *J. Am. Chem. Soc.* **2017**, *139*, 15921–15932.
[68] Y. Dangat, S. Popli, R. B. Sunoj, *J. Am. Chem. Soc.* **2020**, *142*, 17079–17092.
[69] S. Aguado-Ullate, S. Saureu, L. Guasch, J. J. Carbó, *Chem. Eur. J.* **2012**, *18*, 995–1005.
[70] S. Aguado-Ullate, L. Guasch, M. Urbano-Cuadrado, C. Bo, J. J. Carbó, *Catal. Sci. Technol.* **2012**, *2*, 1694.
[71] U. Gellrich, W. Seiche, M. Keller, B. Breit, *Angew. Chem. Int. Ed.* **2012**, *51*, 11033–11038.
[72] C. You, S. Li, X. Li, J. Lan, Y. Yang, L. W. Chung, H. Lv, X. Zhang, *J. Am. Chem. Soc.* **2018**, *140*, 4977–4981.
[73] D. Zhang, J. Wen, X. Zhang, *Chem. Sci.* **2022**, *13*, 7215–7223.
[74] S. Schmidt, G. Abkai, T. Rosendahl, F. Rominger, P. Hofmann, *Organometallics* **2013**, *32*, 1044–1052.
[75] M. Lei, Z. Wang, X. Du, X. Zhang, Y. Tang, *J. Phys. Chem. A* **2014**, *118*, 8960–8970.
[76] C. You, X. Li, Y. Yang, Y. S. Yang, X. Tan, S. Li, B. Wei, H. Lv, L. W. Chung, X. Zhang, *Nat. Commun.* **2018**, *9*, 1–9.
[77] G. te Velde, F. M. Bickelhaupt, E. J. Baerends, C. Fonseca Guerra, S. J. A. van Gisbergen, J. G. Snijders, T. Ziegler, *J. Comput. Chem.* **2001**, *22*, 931–967.
[78] E. van Lenthe, A. Ehlers, E.-J. Baerends, *J. Chem. Phys.* **1999**, *110*, 8943–8953.
[79] C. F. Guerra, J. G. Snijders, G. Velde, E. J. Baerends, *Theor. Chem. Acc.* **1998**, 391–403.
[80] A. D. Becke, *Phys. Rev. A* **1988**, *38*, 3098–3100.
[81] C. Lee, W. Yang, R. G. Parr, *Phys. Rev. B* **1988**, *37*, 785–789.

Manuscript received: April 22, 2022
Revised manuscript received: July 27, 2022
Accepted manuscript online: July 28, 2022
Version of record online: August 19, 2022